

LYAPUNOV AND HALO ORBITS ABOUT L_2

Mischa Kim* and Christopher D. Hall†

We develop and illustrate techniques to obtain periodic orbits around the second Lagrangian point L_2 in the Sun-Earth system based on the Restricted Three-Body Problem. In the case of Lyapunov (planar) orbits, the solutions to the linearized equations of motion allow the generation of the entire family of orbits. For Halo orbits, however, the method of strained coordinates is applied to generate higher-order approximate analytic solutions. Subsequent application of Newton's method improves the initial conditions to obtain periodic solutions to the equations of motions. A graphical user interface has been developed to implement these numerical tools in a user-friendly computational environment.

INTRODUCTION

Renewed interest in studying orbits of spacecraft in the gravitational field generated by more than one body arose in the late 1960s. This study of the behavior of a body with negligible mass in the gravitational field of two bodies with finite mass is well-known and referred to in the literature as the Restricted Three-Body Problem (R3BP).¹ Basic results confirm that in such a system of two massive bodies rotating around their common center of mass in a circular orbit, there exist in the rotating reference frame five equilibrium points of motion, the so-called libration or Lagrangian points, denoted in the literature by L_i , $i = 1, 2, \dots, 5$. The locations of some of these libration points are shown in Figure 1 for two restricted three-body problems.

Such an orbit around L_1 in the Sun-Earth system was chosen for the International Sun-Earth Explorer-3 (ISEE-3), the first spacecraft in a libration point orbit.² Launched on August 12, 1978, ISEE-3 was inserted into its final libration trajectory on November 20, 1978. During its mission, the spacecraft obtained valuable data in solar-wind physics, solar-terrestrial relationship, cosmic-ray physics, and astrophysics. However, the most important contribution of this phase of the ISEE-3 mission could be its exemplification of libration point orbits as prime locations for space missions. As another application, a satellite in a Halo orbit around the translunar libration point L_2 in the Earth-Moon system can be used to assure communication between Earth and the far side of the Moon, if the orbit maintains continuous visibility from Earth.³ The establishment of a bridge for radio communication is a significant problem for future space missions planning to use the far side of the Moon as a launch site for space explorations and as a powerful observation point.

*Graduate of Vienna University of Technology, Vienna, Austria. mikim3@vt.edu

†Associate Professor, Aerospace and Ocean Engineering, Virginia Polytechnic Institute and State University, Blacksburg, Virginia 24061. Associate Fellow AIAA. Member AAS. cdhall@vt.edu

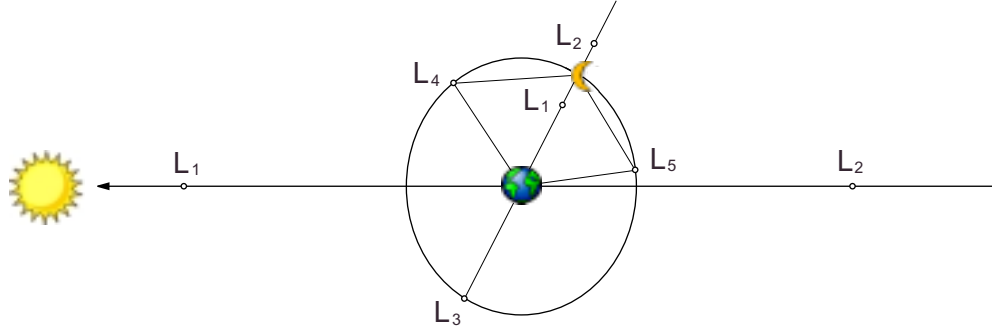


Figure 1: Two restricted three-body problems.

The Solar Heliospheric Observatory (SOHO) was launched on December 2, 1995, which was followed by a two-month cruise to its final destination, the Sun-Earth- L_1 point,² where it was injected into a Halo orbit, on the February 14, 1996. This location was chosen for SOHO because it provides a smooth Sun-spacecraft velocity change throughout the orbit, appropriate for helioseismology. Furthermore, this region lies outside of the magnetosphere, which is required for the “in situ” sampling of the solar wind and its particles. Additionally, the L_1 -vicinity allows permanent observation of the Sun, appropriate for all the investigations.⁴

The Next Generation Space Telescope (NGST)⁵ will orbit around L_2 in the Sun-Earth system. This equilibrium point is ideal for astronomical viewing, since the Sun, Earth, and Moon are always on one side of the telescope. A single shield can eliminate stray light from the Sun and, with some scheduling constraints, from the Earth and Moon. Secondly, the constant distance from the Sun (distance Sun- L_2 $r_{\odot L_2} \approx 1.001$ AU with $1 \text{ AU} \approx 149.6 \times 10^6$ km) provides a stable thermal environment with continuous solar illumination for generating on-board power.

In the last four decades several authors have tried to determine more and more accurate approximations of such equilibrium orbits; these approximate solutions are referred to in the literature as quasi-Halo orbits.⁶ These orbits were first extensively studied by Farquhar^{7,8} and Farquhar and Kamel.⁹ They used the Lindstedt-Poincaré method to determine analytic solutions for these quasiperiodic orbits of the Lagrangian point L_2 in the Earth-Moon system and proved the instability of this orbit family.

In 1973 Hénon presented his paper on vertical stability of periodic orbits in the R3BP.¹⁰ In particular, the stability of planar periodic orbits (Lyapunov orbits) with respect to perturbations perpendicular to the plane were studied.

An in-depth discussion of identified types of motion near the Halo orbit in the center manifold was given by Barden and Howell.¹¹ In particular, they used the invariant subspaces of the monodromy matrix to qualify the nearby motion. An approximation of this nearby motion in the nonlinear center manifold was generated based on the invariant center subspace.

A simple, iterative numerical method for the determination of Halo orbits was developed by

Cielasky and Wie.¹² The nonlinearities inherent to the Halo orbit problem were treated as trajectory-dependent, persistent disturbance inputs. Their method used a disturbance-accommodating linear feedback controller for the computation of a trajectory about an equilibrium point. They also showed that the method can be used as an iterative method for generating a large-amplitude, complex, quasiperiodic Lissajous-trajectory starting with a first-order reference trajectory.

The approach of using two different procedures to obtain an accurate description of the dynamics in an extended neighborhood of the three collinear libration points was suggested by Jorba and Masdemont.¹³ The first method, named the reduction to the center manifold, gave a good description of the dynamics inside the center manifold. Applying the Lindstedt-Poincaré method resulted in approximate formulae for the orbits. Combining these two procedures, Jorba and Masdemont were able to describe and compute solutions in the extended neighborhood of an equilibrium point. They applied this methodology to study the dynamics around the collinear points of the R3BP, with special emphasis on the design of spacecraft trajectories.

Gómez, Masdemont and Simó¹⁴ introduced a method to compute Lissajous orbits on two-dimensional tori around Halo orbits near the collinear libration points in the R3BP. A semianalytical method was applied, based on a Lindstedt-Poincaré procedure, to compute two-dimensional tori around a Halo orbit. They also pointed out that it is possible to obtain Lissajous orbits around Halo orbits after a reduction of the Hamiltonian to the center manifold.¹³ However, this approach was not considered in their paper.

Finally, Giamberardino and Monaco¹⁵ focused on applications of non-linear control techniques to the problem of tracking and maintaining a satellite on prescribed orbits around the translunar libration point L_2 . Due to instability of this equilibrium point, such orbits cannot be maintained without an active control. They compared linear and non-linear methods and concluded that the non-linear controller produced more satisfactory results from the energy consumption point of view. The non-linear controller also turned out to be advantageous in terms of robustness with respect to approximations introduced in the reference determination due to the eccentricity effects.

As the previous discussion shows there exists a vital interest in the research of candidate orbits for future space missions. The present work is focused on the development of algorithms to compute the class of periodic orbits – namely the families of Lyapunov and Halo orbits – around the second Lagrangian point L_2 in the Sun-Earth system. In addition to the other references cited, the first author's *Diplomarbeit*¹⁶ develops the complete details of the work presented in this paper.

THE RESTRICTED THREE-BODY PROBLEM

This section briefly introduces the R3BP for the formulation of the libration point orbit determination.

The Model

As illustrated in Figure 2, the mass m of the third body is negligible compared to the masses of the two primaries ($m_1 > m_2 \gg m$). Hence, the motion of the two massive bodies m_1 and m_2 is obtained from the solution of the two-body problem and is assumed to be a coplanar circular motion

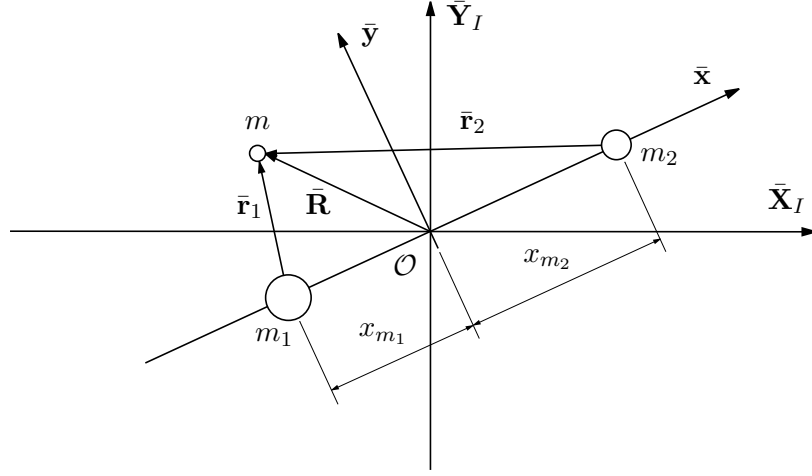


Figure 2: Reference frames.

in the $\bar{\mathbf{X}}_I \bar{\mathbf{Y}}_I$ plane. The rotating reference frame $\{\bar{\mathbf{o}}\} = \{\bar{\mathbf{x}} \ \bar{\mathbf{y}} \ \bar{\mathbf{z}}\}^T$ with origin at the barycenter O of the $m_1 m_2$ system is defined as follows: the vector $\bar{\mathbf{x}}$ points from m_1 to m_2 ; including the vectors $\bar{\mathbf{y}}$ and $\bar{\mathbf{z}}$ these three vectors form a triad such that $\bar{\mathbf{z}} (= \bar{\mathbf{x}} \times \bar{\mathbf{y}})$ is oriented in the direction of the orbital angular velocity ω . The position of the infinitesimal mass m in this reference frame is given by the coordinates \bar{x} , \bar{y} , \bar{z} , and the radius vectors from m_1 to m , m_2 to m and O to m are denoted by \bar{r}_1 , \bar{r}_2 and $\bar{\mathbf{R}}$, respectively. The distance of the two primaries is denoted by r .

Equations of Motion

The derivation of the dimensional equations of motion for the R3BP is well-known. Szebehely¹ is recommended for further reference.

Hence,

$$\begin{aligned} \ddot{\bar{x}} - 2\omega\dot{\bar{y}} - \omega^2\bar{x} &= -G \left(m_1 \frac{\bar{x} + x_{m1}}{\bar{r}_1^3} + m_2 \frac{\bar{x} - x_{m2}}{\bar{r}_2^3} \right), \\ \ddot{\bar{y}} + 2\omega\dot{\bar{x}} - \omega^2\bar{y} &= -G \left(m_1 \frac{\bar{y}}{\bar{r}_1^3} + m_2 \frac{\bar{y}}{\bar{r}_2^3} \right), \\ \ddot{\bar{z}} &= -G \left(m_1 \frac{\bar{z}}{\bar{r}_1^3} + m_2 \frac{\bar{z}}{\bar{r}_2^3} \right). \end{aligned} \quad (1)$$

Introducing the non-dimensional coordinates

$$\bar{\xi} = \frac{\bar{x}}{r}, \quad \bar{\eta} = \frac{\bar{y}}{r}, \quad \bar{\zeta} = \frac{\bar{z}}{r}, \quad \bar{\rho}_{1,2} = \frac{\bar{r}_{1,2}}{r}, \quad (2)$$

and the non-dimensional mass and time units

$$\mu = \frac{m_2}{m_1 + m_2}, \quad \tau = \omega t, \quad (\dot{}) = \frac{d}{dt} = \omega \frac{d}{d\tau} = \omega()' \quad (3)$$

Eqs. (1) become

$$\begin{aligned}
\bar{\xi}'' - 2\bar{\eta}' - \bar{\xi} &= -\frac{(1-\mu)(\bar{\xi} + \mu)}{\bar{\rho}_1^3} - \frac{\mu(\bar{\xi} - 1 + \mu)}{\bar{\rho}_2^3}, \\
\bar{\eta}'' + 2\bar{\xi}' - \bar{\eta} &= -\frac{(1-\mu)\bar{\eta}}{\bar{\rho}_1^3} - \frac{\mu\bar{\eta}}{\bar{\rho}_2^3}, \\
\bar{\zeta}'' &= -\frac{(1-\mu)\bar{\zeta}}{\bar{\rho}_1^3} - \frac{\mu\bar{\zeta}}{\bar{\rho}_2^3}.
\end{aligned} \tag{4}$$

It is not possible to derive analytic solutions for this set of differential equations. However, application of perturbation theory, namely, the *Lindstedt-Poincaré technique*, offers a way to generate approximate initial values α , which can be further used in an adjustment procedure to obtain periodic orbits.

COMPUTATION OF PERIODIC ORBITS

In this section, the methods used to calculate spacecraft trajectories are described. After a brief discussion of the fundamental motions around the collinear equilibrium points approximate values for initial conditions are derived analytically using the method of strained coordinates. Finally, these initial conditions are improved by applying an algorithm based on Newton's method.

Motions in the Vicinity of Collinear Libration Points

Hénon showed that Halo orbits are the result of a bifurcation of Lyapunov orbits and thus do not exist prior to a critical amplitude A_{ξ_c} .¹⁰ Hence, to generate Halo orbits, this bifurcation point, must be identified. The easiest way to achieve this identification is to keep track of the stability of the solutions as they evolve, by monitoring the eigenvalues of the monodromy matrix corresponding to each of the Lyapunov orbits. For any Lyapunov orbit with amplitude less than the critical amplitude, there are four center eigenvalues, one stable eigenvalue ρ_1^s , and one unstable eigenvalue ($\rho_2^u = 1/\rho_1^s$) corresponding to a four-dimensional center manifold, a one-dimensional stable manifold, and a one-dimensional unstable manifold, respectively.¹¹ Of the center eigenvalues, two are real with a value of one ($\rho_i^1 = 1$, $i = 3, 4$), and two others lie on the unit circle and form a complex conjugate pair ($\rho_5^{c.c.} = (\rho_6^{c.c.})^*$). The appearance of a characteristic multiplier with a real value of one with algebraic multiplicity equal to 2 (ρ_i^1 , $i = 3, 4$) is a fundamental property of conservative Hamiltonian systems and is called *non-degenerate* or sometimes *elementary*.¹⁷ Actually this is simply due to the fact that an autonomous Hamiltonian system has a first integral conserving energy.¹⁷ As the amplitude of the individual Lyapunov orbits approach that of the critical orbit, the complex conjugate eigenvalue pair approaches the real value of one along the unit circle. Thus, at the critical amplitude, there are four eigenvalues with a value of one ($\rho_i^1 = 1$, $i = 3, 4, 5, 6$). Within this four-dimensional subspace there are two distinct types of periodic motions. The first type is that of the nearby planar solutions (Lyapunov orbits), and the second type of periodic motion has an out-of-plane component. These are the northern and southern Halo orbits. If the amplitude of the orbit is further increased, the two initially complex eigenvalues start to evolve on the real axes, the value of one of the eigenvalues being the reciprocal value of the other one ($\rho_5^1 = 1/\rho_6^u$). Figure 3 shows the behavior of the eigenvalues just described.

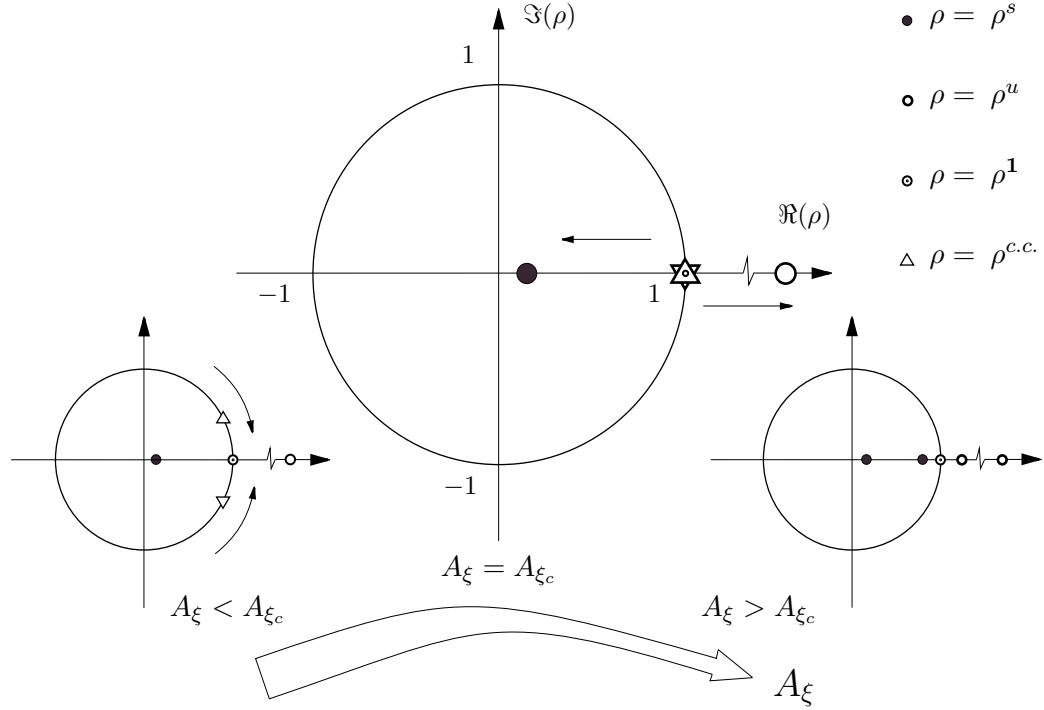


Figure 3: Path of the eigenvalues of the monodromy matrix. ρ^s , ρ^u , ρ^1 , and $\rho^{c.c.}$ are eigenvalues corresponding to a stable, an unstable, a periodic, and a quasi-periodic manifold, respectively.

Obtaining Initial Conditions

As will be shown in the following the knowledge of proper sets of first guesses of initial conditions is of fundamental importance to apply Newton's method successfully. This can be achieved by applying the method of *strained coordinates*, often referred to as the *Lindstedt-Poincaré technique*.¹⁸ The following analysis follows the work of D. L. Richardson,¹⁹ who developed this technique in the 1970s.

For this purpose, the nonlinearities in the equations of motions are expanded into power series of Legendre polynomials. Taking into account the spherical symmetry of solutions around the libration point this expansion can be assumed to be effective. Let

$$\bar{\xi} = \bar{\xi}_0 + \varrho \xi, \quad (5)$$

where $\bar{\xi}_0 = (\bar{\xi}_0, \bar{\eta}_0, \bar{\zeta}_0)^T$ are the coordinates of the equilibrium point, and $\xi = (\xi, \eta, \zeta)^T$ are the components of the position vector of the mass m relative to the equilibrium point. Furthermore, distances are normalized so that the distance between the Earth and L_2 , $r_{\oplus L_2}$, equals one unit, that is

$$\varrho = |\bar{\xi}_0 - (1 - \mu)| = \bar{\rho}_{01}|_{L_2} \equiv \bar{\rho}_{\oplus L_2}. \quad (6)$$

Hence, the non-dimensional equations of motion (4) become

$$\begin{aligned}
\xi'' - 2\eta' - \xi &= -\frac{(1-\mu)\left(\xi + \frac{\bar{\rho}_{\odot L_2}}{\bar{\rho}_{\oplus L_2}}\right)}{\bar{\rho}_{\oplus L_2}^3 \left[\left(\xi + \frac{\bar{\rho}_{\odot L_2}}{\bar{\rho}_{\oplus L_2}}\right)^2 + \eta^2 + \zeta^2\right]^{3/2}} - \frac{\mu(\xi+1)}{\bar{\rho}_{\oplus L_2}^3 [(\xi+1)^2 + \eta^2 + \zeta^2]^{3/2}} \\
&\quad + \frac{\bar{\xi}_0}{\bar{\rho}_{\oplus L_2}}, \\
\eta'' + 2\xi' - \eta &= -\frac{\mu\eta}{\bar{\rho}_{\oplus L_2}^3 [(\xi+1)^2 + \eta^2 + \zeta^2]^{3/2}} - \frac{(1-\mu)\eta}{\bar{\rho}_{\oplus L_2}^3 \left[\left(\xi + \frac{\bar{\rho}_{\odot L_2}}{\bar{\rho}_{\oplus L_2}}\right)^2 + \eta^2 + \zeta^2\right]^{3/2}}, \\
\zeta'' &= -\frac{\mu\zeta}{\bar{\rho}_{\oplus L_2}^3 [(\xi+1)^2 + \eta^2 + \zeta^2]^{3/2}} - \frac{(1-\mu)\zeta}{\bar{\rho}_{\oplus L_2}^3 \left[\left(\xi + \frac{\bar{\rho}_{\odot L_2}}{\bar{\rho}_{\oplus L_2}}\right)^2 + \eta^2 + \zeta^2\right]^{3/2}}.
\end{aligned} \tag{7}$$

where $\bar{\rho}_{\odot L_2} = |\bar{\xi}_0 + \mu| \equiv \bar{\rho}_{0_2}|_{L_2}$ is the normalized distance between the Sun and L_2 . It is straightforward to show that the right-hand sides of Eqs. (7) can be written as partial derivatives, which simplifies Eqs. (7) to

$$\begin{aligned}
\xi'' - 2\eta' - \xi &= \frac{\partial}{\partial \xi} \sum_{l=0}^{\infty} c_l |\xi|^l P_l\left(\frac{\xi}{|\xi|}\right), \\
\eta'' + 2\xi' - \eta &= \frac{\partial}{\partial \eta} \sum_{l=0}^{\infty} c_l |\xi|^l P_l\left(\frac{\xi}{|\xi|}\right), \\
\zeta'' &= \frac{\partial}{\partial \zeta} \sum_{l=0}^{\infty} c_l |\xi|^l P_l\left(\frac{\xi}{|\xi|}\right),
\end{aligned} \tag{8}$$

with

$$c_l = (-1)^l \left(\frac{(1-\mu)\bar{\rho}_{\oplus L_2}^{l-2}}{\bar{\rho}_{\odot L_2}^{l+1}} + \frac{\mu}{\bar{\rho}_{\oplus L_2}^3} \right). \tag{9}$$

In the subsequent application of the method of strained coordinates, only the first three terms in the expansion are considered. One of the basic ideas of this technique is to allow for a frequency correction to avoid secular terms. More explicitly, let

$$\overset{\star}{\tau} = \Omega\tau, \quad ()' = \frac{d}{d\tau} = \frac{d\overset{\star}{\tau}}{d\tau} \frac{d}{d\overset{\star}{\tau}} = \Omega \frac{d}{d\overset{\star}{\tau}} = \Omega ()^{\star}, \tag{10}$$

where

$$\Omega = 1 + \sum_{i=1}^{\infty} \epsilon^i \Omega_i. \tag{11}$$

Furthermore it is assumed that the final solution to the equations of motion can be represented in the form

$$\xi(\overset{\star}{\tau}) = \sum_{i=1}^{\infty} \epsilon^i \xi_i(\overset{\star}{\tau}), \tag{12}$$

where $\xi_1(\overset{\star}{\tau})$ indicates the solution to the linearized equations of motion. As aforementioned only the first three terms in the power series expansion are considered, that is, Eqs. (8) are approximated

by

$$\begin{aligned}
\Omega^2 \xi^{**} - 2\Omega \eta^* - \xi &= 2c_2 \xi + \frac{3}{2}c_3(2\xi^2 - \eta^2 - \zeta^2) + 2c_4(2\xi^2 - 3\eta^2 - 3\zeta^2)\xi, \\
\Omega^2 \eta^{**} + 2\Omega \xi^* - \eta &= -c_2 \eta - 3c_3 \xi \eta - \frac{3}{2}c_4(4\xi^2 - \eta^2 - \zeta^2)\eta, \\
\Omega^2 \zeta^{**} &= c_2 \zeta - 3c_3 \xi \zeta - \frac{3}{2}c_4(4\xi^2 - \eta^2 - \zeta^2)\zeta.
\end{aligned} \tag{13}$$

Considering Eqs. (11) and (12) it is easy to show that the solutions to the equations of motion of first order in ϵ can be obtained as

$$\begin{aligned}
\xi_1(\tau^*) &= -A_\xi \cos \tau_{\xi\eta}^*, \\
\eta_1(\tau^*) &= k A_\xi \sin \tau_{\xi\eta}^*, \\
\zeta_1(\tau^*) &= A_\zeta \sin \tau_\zeta^*,
\end{aligned} \tag{14}$$

where

$$\tau_{\xi\eta}^* = \omega_{\xi\eta} \tau^* + \phi_{\xi\eta}, \quad \text{and} \quad \tau_\zeta^* = \omega_{\xi\eta} \tau^* + \phi_\zeta. \tag{15}$$

Setting $\tau^* = 0$ in Eqs. (14) provides approximate values for initial conditions for small-amplitude Lyapunov orbits. However, for Halo orbits calculation of such first guesses require higher-order terms to be considered. Thus, the next step is to replace in the $\mathcal{O}(\epsilon^2)$ equations these solutions to obtain the next order approximation

$$\begin{aligned}
\xi_2^{**} - 2\eta_2^* - (1 + c_2)\xi_2 &= 2\Omega_1 \omega_{\xi\eta} A_\xi (k - \omega_{\xi\eta}) \cos \tau_{\xi\eta}^* + \alpha_\xi^{20} \\
&\quad + \alpha_\xi^{21} \cos(2\tau_{\xi\eta}^*) + \alpha_\xi^{22} \cos(2\tau_\zeta^*), \\
\eta_2^{**} + 2\xi_2^* - (1 - c_2)\eta_2 &= 2\Omega_1 A_\xi \omega_{\xi\eta} (k\omega_{\xi\eta} - 1) \sin \tau_{\xi\eta}^* + \alpha_\eta^{20} \sin(2\tau_{\xi\eta}^*), \quad \ddagger \\
\zeta_2^{**} + \omega_{\xi\eta}^2 \zeta_2^* &= 2\Omega_1 A_\zeta \omega_{\xi\eta}^2 \sin \tau_\zeta^* + \alpha_\zeta^{20} \sin(\tau_{\xi\eta}^* + \tau_\zeta^*) \\
&\quad + \alpha_\zeta^{20} \sin(\tau_\zeta^* - \tau_{\xi\eta}^*).
\end{aligned} \tag{16}$$

In Eqs. (16) the $\cos \tau_{\xi\eta}^*$, $\sin \tau_{\xi\eta}^*$ and $\sin \tau_\zeta^*$ expressions generate secular terms and thus have to be removed. This can be achieved by setting $\Omega_1 = 0$. The solution to the $\mathcal{O}(\epsilon^2)$ -equations of motion can then be written as

$$\begin{aligned}
\xi_2(\tau^*) &= a_\xi^{20} + a_\xi^{21} \cos(2\tau_{\xi\eta}^*) + a_\xi^{22} \cos(2\tau_\zeta^*), \\
\eta_2(\tau^*) &= a_\eta^{20} \sin(2\tau_{\xi\eta}^*) + a_\eta^{21} \sin(2\tau_\zeta^*), \\
\zeta_2(\tau^*) &= a_\zeta^{20} \sin(\tau_{\xi\eta}^* + \tau_\zeta^*) + a_\zeta^{21} \sin(\tau_\zeta^* - \tau_{\xi\eta}^*).
\end{aligned} \tag{17}$$

Obviously the $\mathcal{O}(\epsilon^2)$ -approximation does not yield a frequency correction since $\Omega_1 = 0$, so the third order equations have to be considered. Thus the following system of differential equations has

[‡]Remark: α_{dir}^{ij} is the j th constant in the i th-order approximation in the *dir*-equation of the EOM.

to be solved

$$\begin{aligned}
\xi_3^{**} - 2\eta_3^* - (1 + c_2)\xi_3 &= [\psi_1 + 2\Omega_2\omega_{\xi\eta}A_\xi(k - \omega_{\xi\eta})] \cos \tau_{\xi\eta}^* + \alpha_\xi^{23} \cos(3\tau_{\xi\eta}^*) \\
&\quad + \alpha_\xi^{24} \cos(\tau_{\xi\eta}^* + 2\tau_\zeta^*) + \alpha_\xi^{25} \cos(2\tau_\zeta^* - \tau_{\xi\eta}^*), \\
\eta_3^{**} + 2\xi_3^* - (1 - c_2)\eta_3 &= [\psi_2 + 2\Omega_2\omega_{\xi\eta}A_\xi(k\omega_{\xi\eta} - 1)] \sin \tau_{\xi\eta}^* + \alpha_\eta^{21} \sin(3\tau_{\xi\eta}^*) \\
&\quad + \alpha_\eta^{22} \sin(\tau_{\xi\eta}^* + 2\tau_\zeta^*) + \alpha_\eta^{23} \sin(2\tau_\zeta^* - \tau_{\xi\eta}^*), \\
\zeta_3^{**} + \omega_{\xi\eta}^2 \zeta_3^* &= [\psi_3 + A_\zeta(2\Omega_2\omega_{\xi\eta}^2 + \delta/\epsilon^2)] \sin \tau_\zeta^* + \alpha_\zeta^{21} \sin(3\tau_\zeta^*) \\
&\quad + \alpha_\zeta^{22} \sin(2\tau_{\xi\eta}^* + \tau_\zeta^*) + \alpha_\zeta^{23} \sin(2\tau_{\xi\eta}^* - \tau_\zeta^*),
\end{aligned} \tag{18}$$

which yields for the $\mathcal{O}(\epsilon^3)$ solution

$$\begin{aligned}
\xi_3(\tau^*) &= a_\xi^{30} \cos(3\tau_{\xi\eta}^*), \\
\eta_3(\tau^*) &= a_\eta^{30} \sin(3\tau_{\xi\eta}^*) + a_\eta^{31} \sin \tau_{\xi\eta}^*, \\
\zeta_3(\tau^*) &= a_\zeta^{31} \cos(3\tau_{\xi\eta}^*).
\end{aligned} \tag{19}$$

The complete solution of third order is then obtained as

$$\begin{aligned}
\xi(\tau^*) &= -A_\xi \cos \tau_{\xi\eta}^* + a_\xi^{20} A_\xi^2 + a_\xi^{21} A_\zeta^2 \\
&\quad + (a_\xi^{22} A_\xi^2 - a_\xi^{23} A_\zeta^2) \cos(2\tau_{\xi\eta}^*) + (a_\xi^{30} A_\xi^3 - a_\xi^{31} A_\xi A_\zeta^2) \cos(3\tau_{\xi\eta}^*), \\
\eta(\tau^*) &= kA_\xi \sin \tau_{\xi\eta}^* + (a_\eta^{20} A_\xi^2 - a_\eta^{21} A_\zeta^2) \sin(2\tau_{\xi\eta}^*) \\
&\quad + (a_\eta^{30} A_\xi^3 - a_\eta^{31} A_\xi A_\zeta^2) \sin(3\tau_{\xi\eta}^*) + (a_\eta^{32} A_\xi^3 + (a_\eta^{33} - a_\eta^{34}) A_\xi A_\zeta^2) \sin \tau_{\xi\eta}^*, \\
\zeta(\tau^*) &= A_\zeta \cos \tau_{\xi\eta}^* + a_\zeta^{20} A_\xi A_\zeta \cos(2\tau_{\xi\eta}^* - 3) + (a_\zeta^{31} A_\xi^2 A_\zeta - a_\zeta^{30} A_\zeta^3) \cos(3\tau_{\xi\eta}^*).
\end{aligned} \tag{20}$$

First guesses of initial conditions for Halo orbits obtained by setting $\tau^* = 0$ are sufficiently close to the exact initial conditions so that Newton's method shows expected convergence.

Adjusting Initial Conditions

With the approximated initial conditions calculated using Eqs. (14) and (20) for small-amplitude Lyapunov orbits and Halo orbits, respectively, these values are corrected using an algorithm based on Newton's method. For the following discussion we denote by α the so-called orbit setup vector, whose components are – for the time being – equal to the initial conditions[§]. In addition, we denote by $\alpha_{ext} = (\alpha, T)^T$ the extended orbit setup vector, considering the fact that the orbit period T is another unknown in the iteration procedure. Thus, let $\varphi(\alpha, t)$ be a solution to the differential equations (8) for a given orbit setup. It is obvious, that

$$\mathbf{g}(\alpha_{ext}) = \varphi(\alpha, t_0 + T) - \alpha = \mathbf{0} \tag{21}$$

[§]The distinction between the orbit setup vector and the vector of initial conditions will become clear throughout the analysis.

has to hold for a periodic solution trajectory. Thus, with an initial guess $\tilde{\alpha}_{ext}$ let

$$\alpha_{ext} = \tilde{\alpha}_{ext} + \delta\alpha_{ext} . \quad (22)$$

The Taylor series expansion of $\mathbf{g}(\tilde{\alpha}_{ext} + \delta\alpha_{ext})$ then results

$$\mathbf{g}(\alpha_{ext}) = \mathbf{g}(\tilde{\alpha}_{ext}) + \left. \frac{\partial \mathbf{g}(\alpha_{ext})}{\partial \alpha_{ext}} \right|_{\alpha_{ext}=\tilde{\alpha}_{ext}} \delta\alpha_{ext} + \mathcal{O}(\delta\alpha_{ext}^2) . \quad (23)$$

Provided that $\|\mathbf{g}(\alpha_{ext})\| < \|\mathbf{g}(\tilde{\alpha}_{ext})\|$ ($\Rightarrow \mathbf{g}(\alpha_{ext}) = \mathbf{0}$) and considering only the linear term in the Taylor series, the *Newton step* $\delta\alpha_{ext}$ is derived as

$$\delta\alpha_{ext} = - \left[\left. \frac{\partial \mathbf{g}(\alpha_{ext})}{\partial \alpha_{ext}} \right|_{\alpha_{ext}=\tilde{\alpha}_{ext}} \right]^{-1} \mathbf{g}(\tilde{\alpha}_{ext}) , \quad (24)$$

which allows one to improve the initial guess to

$$\tilde{\alpha}_{ext} \rightarrow \delta\alpha_{ext} + \tilde{\alpha}_{ext} . \quad (25)$$

Applying Eqs. (24) and (25) in an iterative fashion, this method shows a quadratic convergence to improved values for α_{ext} .

Taking into account the symmetry of the R3BP, choosing a point on the \bar{x} -axis (Figure 1) as the starting point to numerically generate the trajectory $\varphi(\alpha, t)$ entails, that for Lyapunov orbits the trajectory is uniquely defined by $\alpha_{ext} = (\eta^*(0), T)^T$ and the orbit amplitude $A_\xi \equiv \xi(0)$, which we choose as the system parameter. Thus, the Newton step for Lyapunov orbits yields

$$\begin{pmatrix} \delta\eta^*(0) \\ \delta T \end{pmatrix} = - \left[\left. \frac{\partial(\mathbf{g}_\eta(\alpha_{ext}), \mathbf{g}_{\eta^*}(\alpha_{ext}))}{\partial(\eta^*(0), T)} \right|_{\alpha_{ext}=\tilde{\alpha}_{ext}} \right]^{-1} \begin{pmatrix} \mathbf{g}_\eta(\tilde{\alpha}_{ext}) \\ \mathbf{g}_{\eta^*}(\tilde{\alpha}_{ext}) \end{pmatrix} , \quad (26)$$

where the $\mathbf{g}_{dir}(\alpha_{ext})$ are the components in the *dir*-directions of the $\mathbf{g}(\alpha_{ext})$ vector. In the case of Halo orbits, similar arguments result for the extended orbit setup vector $\alpha_{ext} = (\zeta(0), \eta^*(0), T)^T$, choosing $A_\xi \equiv \xi(0)$ as the system parameter[¶]. Hence, the Newton step for Halo orbits becomes

$$\begin{pmatrix} \delta\zeta(0) \\ \delta\eta^*(0) \\ \delta(T/2) \end{pmatrix} = - \left[\left. \frac{\partial(\mathbf{g}_\eta(\alpha_{ext}), \mathbf{g}_{\xi^*}(\alpha_{ext}), \mathbf{g}_{\zeta^*}(\alpha_{ext}))}{\partial(\zeta(0), \eta^*(0), T/2)} \right|_{\alpha_{ext}=\tilde{\alpha}_{ext}} \right]^{-1} \begin{pmatrix} \mathbf{g}_\eta(\tilde{\alpha}_{ext}) \\ \mathbf{g}_{\xi^*}(\tilde{\alpha}_{ext}) \\ \mathbf{g}_{\zeta^*}(\tilde{\alpha}_{ext}) \end{pmatrix} . \quad (27)$$

As aforementioned, Eqs. (14) provide proper sets of initial conditions for small-amplitude Lyapunov orbits, only. However, once a periodic orbit is calculated, the whole family of Lyapunov orbits can be obtained by choosing an *Euler-Newton step*²⁰ as the first step in the Newton iteration to generate orbits with gradually increasing amplitude. To this end, Eq. (21) is rewritten as

$$\mathbf{g}(\alpha_{ext}, A_\xi) = \mathbf{0} . \quad (28)$$

[¶]Note: The optimal value for Δx appearing in numerical calculations of derivatives $g(x)' \approx \frac{\Delta g(x)}{\Delta x} = \frac{g(x+\Delta x/2) - g(x-\Delta x/2)}{\Delta x}$ is given by²⁰ $\Delta x = eps^{1/3} \max\{|x|, typ\ x\} sign(x)$, where *eps* is the machine epsilon.

[¶]It is obvious, that in the case given a specific orbit amplitude A_ζ rather than A_ξ the iteration algorithm can be conducted in the exact same way by exchanging $\xi(0) \longleftrightarrow \zeta(0)$ in Eq. (27).

Let

$$A_\xi = \tilde{A}_\xi + \delta A_\xi, \quad (29)$$

the Taylor series expansion of $\mathbf{g}(\boldsymbol{\alpha}_{ext}, A_\xi)$ results

$$\begin{aligned} \mathbf{g}(\boldsymbol{\alpha}_{ext}, A_\xi) = & \mathbf{g}(\tilde{\boldsymbol{\alpha}}_{ext}, \tilde{A}_\xi) + \frac{\partial \mathbf{g}(\boldsymbol{\alpha}_{ext}, A_\xi)}{\partial \boldsymbol{\alpha}_{ext}} \Big|_{\substack{\boldsymbol{\alpha}_{ext} = \tilde{\boldsymbol{\alpha}}_{ext} \\ A_\xi = \tilde{A}_\xi}} \delta \boldsymbol{\alpha}_{ext} + \\ & + \frac{\partial \mathbf{g}(\boldsymbol{\alpha}_{ext}, A_\xi)}{\partial A_\xi} \Big|_{\substack{\boldsymbol{\alpha}_{ext} = \tilde{\boldsymbol{\alpha}}_{ext} \\ A_\xi = \tilde{A}_\xi}} \delta A_\xi + \mathcal{O}(\delta \boldsymbol{\alpha}_{ext}^2, \delta A_\xi^2). \end{aligned} \quad (30)$$

With $\mathbf{g}(\tilde{\boldsymbol{\alpha}}_{ext}, \tilde{A}_\xi) = \mathbf{0}$ describing the initial periodic orbit, setting the left hand side of Eq. (30) equal to zero and disregarding all terms of $\mathcal{O}(\delta \boldsymbol{\alpha}_{ext}^2, \delta A_\xi^2)$, the *Euler-Newton step* yields

$$\begin{aligned} \begin{pmatrix} \delta \eta^*(0) \\ \delta T \end{pmatrix} = & - \left\{ \left[\frac{\partial(\mathbf{g}_\eta(\boldsymbol{\alpha}_{ext}, A_\xi), \mathbf{g}_{\eta^*}(\boldsymbol{\alpha}_{ext}, A_\xi))}{\partial(\eta^*(0), T)} \right]^{-1} \times \right. \\ & \left. \left(\frac{\partial(\mathbf{g}_\eta(\boldsymbol{\alpha}_{ext}, A_\xi), \mathbf{g}_{\eta^*}(\boldsymbol{\alpha}_{ext}, A_\xi))}{\partial A_\xi} \right) \right\} \Big|_{\substack{\boldsymbol{\alpha}_{ext} = \tilde{\boldsymbol{\alpha}}_{ext} \\ A_\xi = \tilde{A}_\xi}} \delta A_\xi. \end{aligned} \quad (31)$$

This section introduced techniques to compute the family of Lyapunov orbits and Halo orbits about L_2 in the Sun-Earth system. The implementation of a Graphical User Interface allows to easily perform these calculations and access the resulting spacecraft trajectories.

IMPLEMENTATION OF A GRAPHICAL USER INTERFACE

The development of a Graphical User Interface (GUI) is helpful in providing straightforward access to numerical and graphical representations of libration point orbits. As illustrated in Figure 4 the interface is easy to use. There are two ways to enter data into the program. Using the **Load data** button the user can load a preexisting data file of type `datafile.bin`. Loading a data file causes the data to appear in the text boxes labeled Orbit data (dim.) and Initial values (nondim.), but does not calculate the orbit. The other option is to type the amplitude of the orbit into the text box labeled Amplitude. The user can also choose a specific orbit setup. The parameter specifying the orbit (x - or z -amplitude) and the orbit type can be changed (Northern or Southern Halo orbit, Lyapunov orbit). Note that the unit appearing in the popup menu Units is also used to scale the plots. The **Plot** button causes the program to calculate and plot the requested orbit as three two-dimensional graphs, corresponding to the zy -, zx -, and the xy -projections, respectively. Initial conditions are indicated in these plots with a black triangle, and L_2 is represented by a blue star. Having computed a particular orbit, its data set can then be saved using the **Save data** button. Subsequent plotting of different orbits allows easy comparison of the effects of varying amplitude. This feature might be advantageous if different orbits are to be compared. The **Clear** button clears all graphics.

Planned improvements of the GUI will include the ability to change the amplitude interactively by simply dragging the mouse over the graphical screen, thus being able to observe the change of the shape of the orbit in real time. For that purpose, the parametric expressions describing the

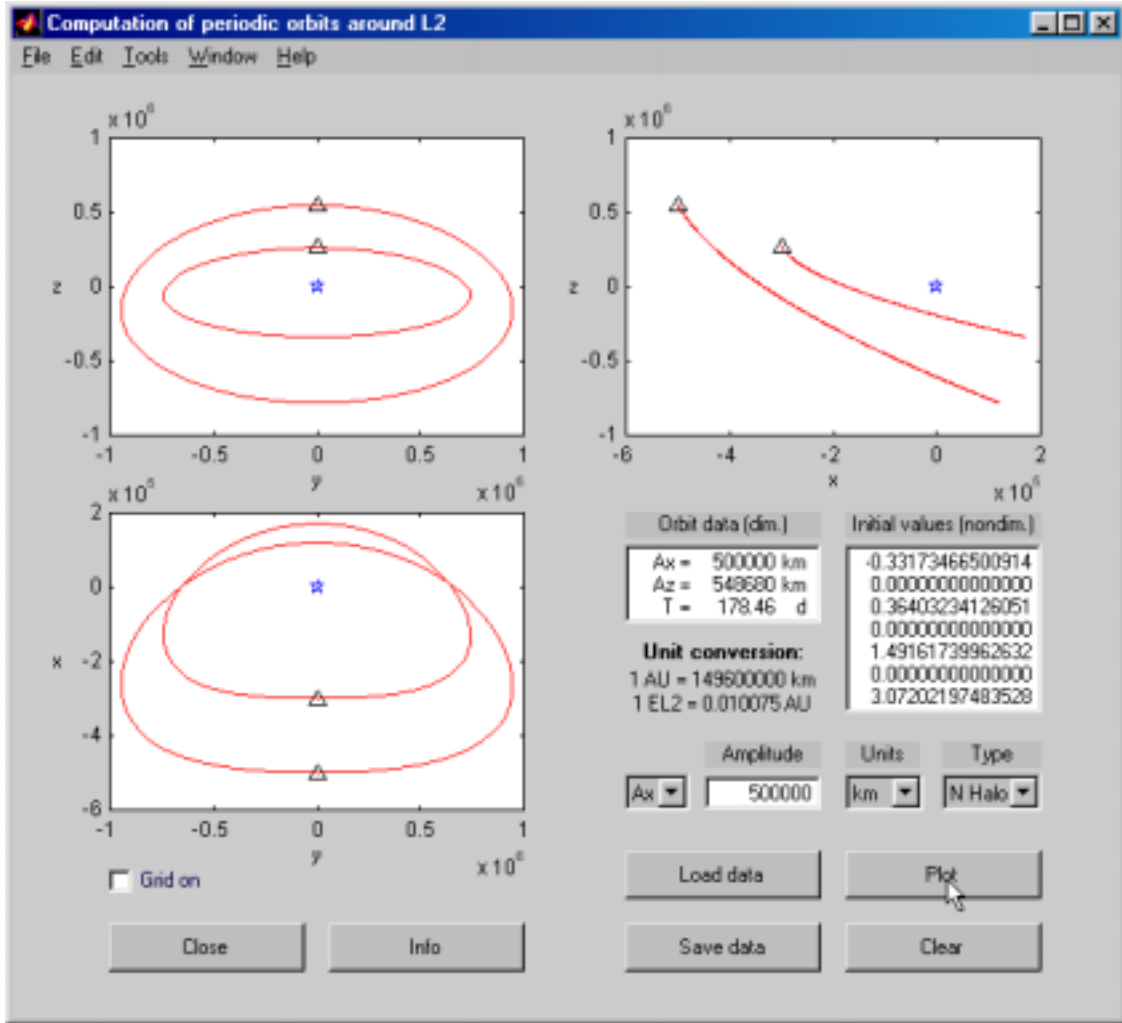


Figure 4: The Graphical User Interface.

approximate initial conditions of the orbits can be used in combination with Eqs. (20) to obtain orbits analytically. Once a particular orbit setup is chosen these approximate initial conditions can then be adjusted to obtain the optimal spacecraft trajectory as described above.

RESULTS

The iterative generation of the family of Lyapunov orbits to finally obtain the requested orbit can be quite time-consuming. For this reason a calculation of some orbits of the family of Lyapunov orbits is used to obtain parametric expressions in the form of

$$\eta^*(0) = f_{L,\eta^*}(A_\xi) \quad \text{and} \quad T = f_{L,T}(A_\xi). \quad (32)$$

Figures 5 and 6 show the graphical plots for polynomials of degree 7 for both families of Lyapunov and Halo orbits. These polynomials can be obtained in a straightforward manner using MATLAB. The polynomials provide first guesses of initial conditions which are significantly more accurate than are those obtained from Eqs. (14) and (20).

A comparison of iteration histories of first guesses obtained by the Lindstedt-Poincaré technique and polynomial fitting curves for two orbits is shown in Tables 1 and 2. As can be seen, the polynomials provide a first guess of initial conditions that yields results of arbitrary accuracy after fewer iteration steps when compared to the application of the Lindstedt-Poincaré technique. The difference in performance becomes increasingly obvious as the amplitude of the orbit is increased. For a Halo orbit of amplitude $A_x = 500,000$ km the number of iteration steps differs by a factor of four to reach a tolerance of $tol = 5 \times 10^{-15}$. In the following tables and figures some sample orbits obtained using this technique are presented.

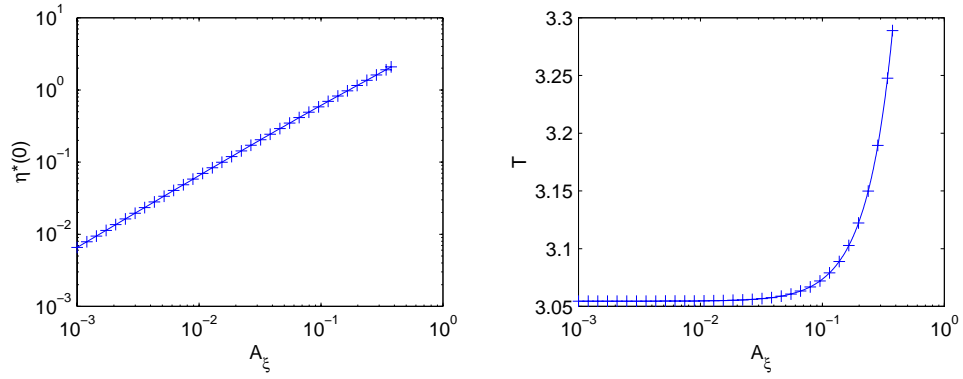


Figure 5: Polynomials describing initial conditions of Lyapunov orbits.

Table 1: Comparison of iteration histories of a first guess for initial conditions for a Halo orbits of amplitude $A_x = 350,000$ km obtained by the Lindstedt-Poincaré technique and polynomial fitting curves.

A_x	n	$\ \mathbf{g}(\boldsymbol{\alpha}_{ext})\ $ after n iteration steps using	
		Lindstedt-Poincaré	polynomial
350,000 km	0	$3.1200525853 \times 10^{-2}$	$6.8814598988 \times 10^{-13}$
	1	$5.8999018953 \times 10^{-3}$	$2.9658068733 \times 10^{-14}$
	2	$9.6845174584 \times 10^{-5}$	$1.9314531705 \times 10^{-15}$
	3	$5.4837859251 \times 10^{-8}$	
	4	$3.5484464441 \times 10^{-15}$	

Figure 7 shows sample Lyapunov orbits with amplitudes in the range of $A_x = 560$ km and $A_x = 560,000$ km. For small amplitude orbits the solution trajectory shows the typical shape obtained as a superposition of sine- and cosine functions. This behaviour is described by the solution to the linearized equations of motions (14), with $\zeta_1(\tau^*) \equiv 0$ for all τ^* . Increasing the amplitude

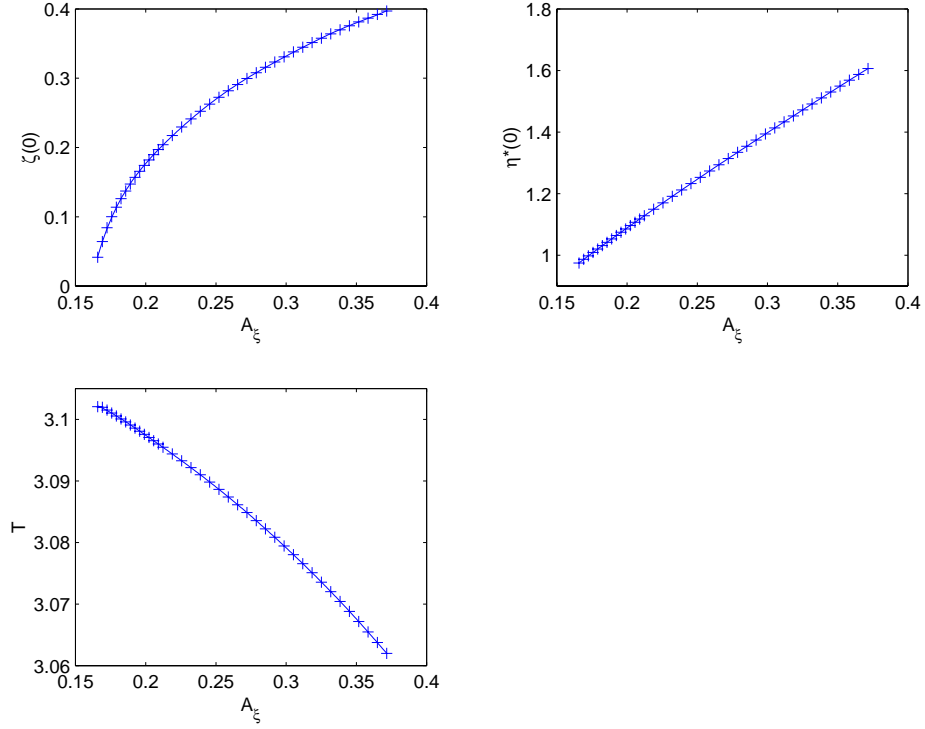


Figure 6: Polynomials describing initial conditions of Halo orbits.

Table 2: Comparison of iteration histories of a first guess for initial conditions for a Halo orbits of amplitude $A_x = 500,000$ km obtained by the Lindstedt-Poincaré technique and polynomial fitting curves.

A_x	n	$\ \mathbf{g}(\boldsymbol{\alpha}_{ext})\ $ after n iteration steps using	
		Lindstedt-Poincaré	polynomial
500,000 km	0	$3.6484180352 \times 10^{-1}$	$5.6972164581 \times 10^{-14}$
	1	$3.4557259625 \times 10^{-2}$	$7.9922236956 \times 10^{-15}$
	2	$2.8191846560 \times 10^{-4}$	$7.3073229310 \times 10^{-16}$
	3	$1.7856647485 \times 10^{-6}$	
	4	$7.1290885140 \times 10^{-13}$	
	5	$2.2413517073 \times 10^{-14}$	
	6	$1.6379283987 \times 10^{-14}$	
	7	$9.6817763917 \times 10^{-15}$	
	8	$6.1639079922 \times 10^{-15}$	
	9	$4.3326830472 \times 10^{-15}$	

significantly results a dramatic change in shape of the spacecraft orbit.

Using polynomials to obtain initial conditions offers the possibility to choose either one of the orbit amplitudes (A_x , A_z) or the period T as the specifying parameter to generate the spacecraft trajectories. Figures 8 and 9 show Halo orbits of similar amplitude-range. The former was generated using A_x as the determining parameter, whereas for the latter the amplitude in the z -direction, A_z , was chosen as the specifying parameter.

Barden and Howell¹¹ describe the dynamics in the center manifold of the R3BP by means of Dynamical System Theory (DST). It is shown that Halo orbits do not exist prior to a minimum amplitude ($A_{x_{min}} \approx 2.1 \times 10^5$ km). This can be anticipated by studying Figure 9, orbits with decreasing amplitude tend to straighten out and tilt back into the Sun-Earth rotational plane.

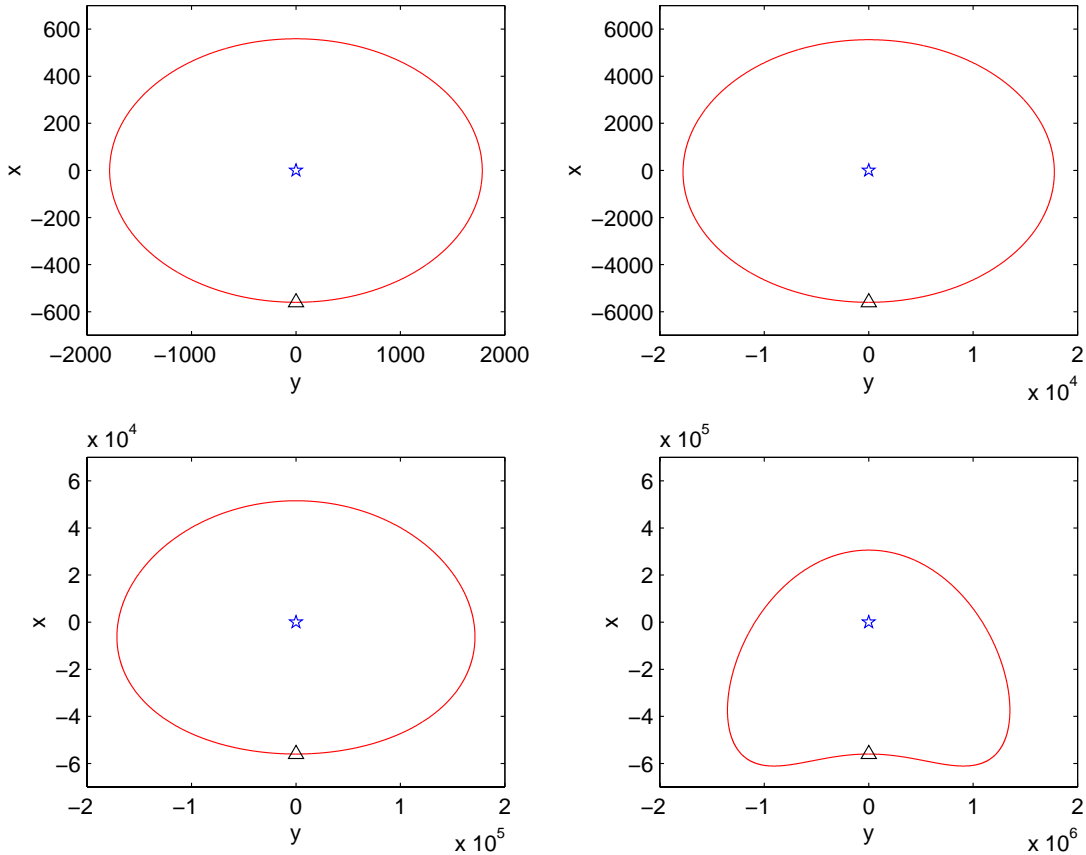


Figure 7: Four Lyapunov orbits with amplitudes in between $A_x = 560$ km (upper left Figure) and $A_x = 560,000$ km (lower right Figure). Initial conditions are indicated with a triangle, L_2 is represented by a star.

SUMMARY AND CONCLUSIONS

An algorithm for the numerical computation of both families of periodic orbits around the second Lagrangian point in the Sun-Earth system, namely the family of Lyapunov orbits and the family

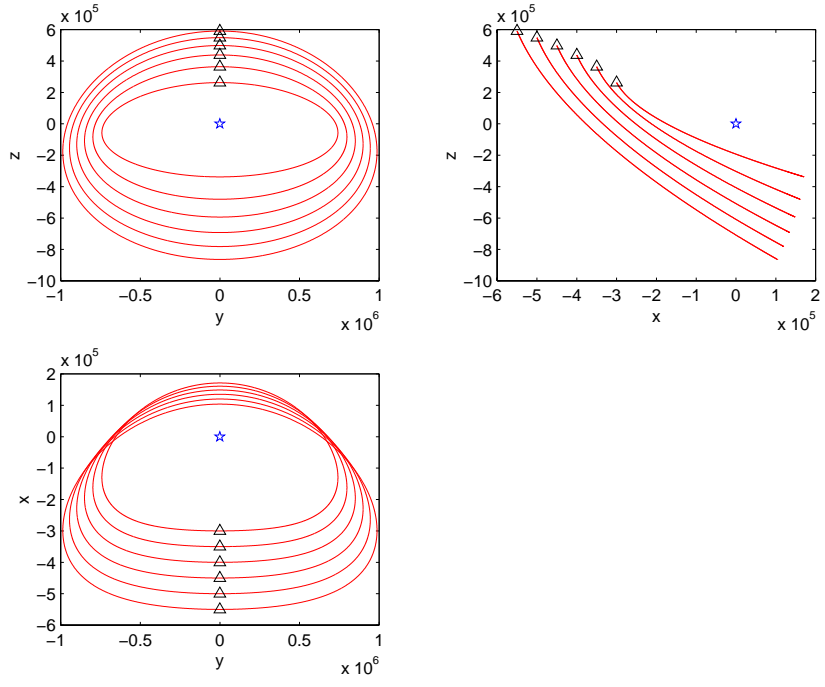


Figure 8: Six northern Halo orbits with amplitudes in between $A_x = 3 \times 10^5$ km and $A_x = 5.5 \times 10^5$ km. Initial conditions are indicated with a triangle, L_2 is represented by a star.

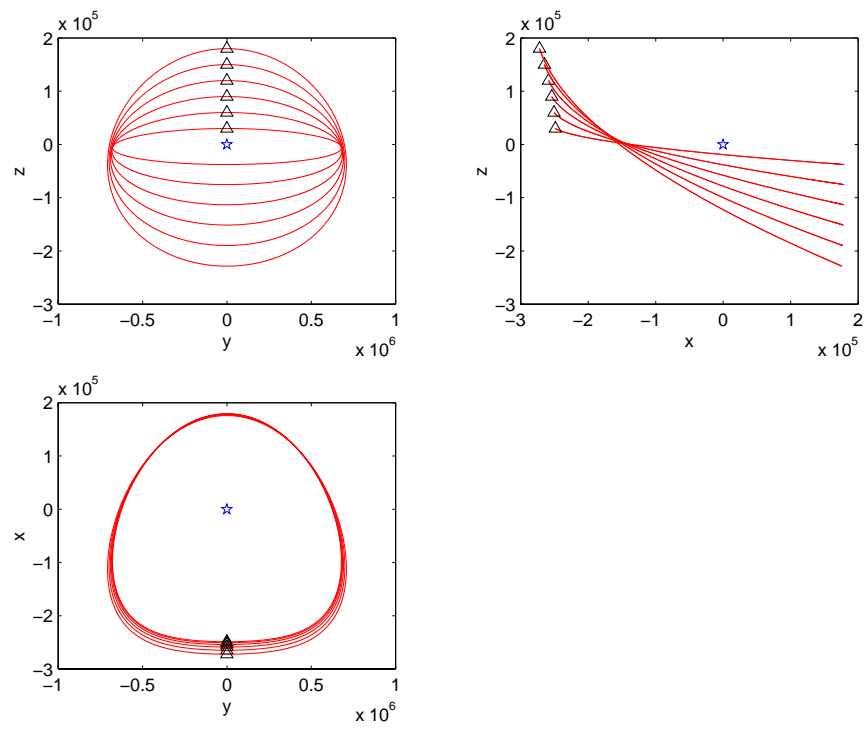


Figure 9: Six northern Halo orbits with amplitudes in between $A_z = 3 \times 10^4$ km and 18×10^4 km. Initial conditions are indicated with a triangle, L_2 is represented by a star.

of Halo orbits is presented. It is shown that the solution to the linearized equations of motion can provide insight to the behavior of the system only in the immediate vicinity of the libration point, as nonlinearities are disregarded. As one of the fundamental results of the discussion, the importance of finding reasonable first guesses of initial conditions in order to guarantee the convergence of the correction algorithm is pointed out. For Lyapunov orbits the solutions to the linearized equations of motion offer first guesses sufficiently close to the initial conditions. In the case of Halo, however, refined approximations using the Lindstedt-Poincaré technique are needed. However, parametric expressions for these initial conditions in the form of polynomials turns out to be significantly more accurate and are useful in establishing an effective routine for interactively computing Lyapunov and Halo orbits. These algorithms have been integrated into an interactive Matlab code with a user-friendly Graphical User Interface.

ACKNOWLEDGMENTS

This research was motivated by NASA Goddard's Submillimeter Probe of Early Cosmic Structure (SPECS) project, and the authors are grateful to David Leisawitz for many useful conversations. The first author was partially supported by the Botstiber Foundation while completing his *Diplomarbeit* at Virginia Tech. The second author was supported by the Air Force Office of Scientific Research.

References

- [1] Szebehely, V., *Theory of Orbits – The Restricted Problem of Three Bodies*, Academic Press, New York, 1967.
- [2] Farquhar, R. W., "Halo-Orbit and Lunar-Swingby Missions of the 1990s," *Acta Astronautica*, Vol. 24, 1991, pp. 227–234.
- [3] Breakwell, J. V., Kamel, A. A., and Ratner, M. J., "Station Keeping for a Translunar Communication Station," *Celestial Mechanics*, Vol. 10, 1974, pp. 357–373.
- [4] Huber, M., Bonnet, R., Dale, D., Arduini, M., Fröhlich, C., Domingo, V., and Whitcomb, G., "The History of the SOHO Mission," *ESA Bulletin*, Vol. 86, May 1996, pp. 25–35.
- [5] Dressler, A., "Hubble and Beyond Report, Exploration and the Search for Origins: A Vision for Ultraviolet-Optical-Infrared Space Astronomy," Tech. rep., Association of Universities for Research in Astronomy, Washington D.C., 1996.
- [6] Giamberardino, P. D. and Monaco, S., "Nonlinear Regulation in Halo Orbits Control Design," *In Proceedings 31st IEEE Decision and Control Conference*, Tucson, U.S.A., 1992, pp. 536–541.
- [7] Farquhar, R. W., "The Control and Use of Libration-Point Satellites," *NASA-TR-R-346*, September 1970.
- [8] Farquhar, R. W., "The Utilization of Halo Orbits in Advanced Lunar Operations," *NASA-TN-D-6365*, July 1971.

- [9] Farquhar, R. W. and Kamel, A. A., “Quasi-Periodic Orbits About the Translunar Libration Point,” *Celestial Mechanics*, Vol. 7, 1973, pp. 458–473.
- [10] Hénon, M., “Vertical Stability of Periodic Orbits in the Restricted Problem,” *Astronomy and Astrophysics*, Vol. 28, 1973, pp. 415–426.
- [11] Barden, B. T. and Howell, K. C., “Fundamental Motions Near Collinear Libration Points and Their Transitions,” *The Journal of the Astronautical Sciences*, Vol. 46, No. 4, October-December 1998, pp. 361–378.
- [12] Cielasky, D. and Wie, B., “New Approach to Halo Orbit Determination and Control,” *Journal of Guidance, Control and Dynamics*, Vol. 19, No. 2, March-April 1996, pp. 266–273.
- [13] Jorba, A. and Masdemont, J., “Dynamics in the Center Manifold of the Collinear Points of the Restricted Three Body Problem,” *Physica D*, Vol. 132, 1999, pp. 189–213.
- [14] Gómez, G., Masdemont, J., and Simó, C., “Lissajous Orbits Around Halo Orbits,” *Advances in astronautical sciences*, Vol. 95, No. 1, 1997, pp. 117–134.
- [15] Giamberardino, P. D. and Monaco, S., “On Halo Orbits Spacecraft Stabilization,” *Acta Astronautica*, Vol. 38, No. 12, 1996, pp. 903–925.
- [16] Kim, M., “Periodic Spacecraft Orbits for Future Space-based Deep Space Observations,” Tech. rep., Vienna Institute of Technology, Vienna, Austria, 2001.
- [17] Meyer, K. R., *Periodic Solutions of the N-Body Problem*, Springer-Verlag, Berlin, 1999.
- [18] Nayfeh, A., *Perturbation Methods*, Pure and applied mathematics, Wiley, New York, 1973.
- [19] Richardson, D. L., “Analytic Construction of Periodic Orbits About the Collinear Points,” *Celestial Mechanics*, Vol. 22, 1980, pp. 241–253.
- [20] Dennis, J. E. and Schnabel, R. B., *Numerical Methods for Unconstrained Optimization and Nonlinear Equations*, Prentice-Hall, Englewood Cliffs, New Jersey, 1983.